Cell Host & Microbe
Article

Structural Basis of HIV-1 Tethering to Membranes by the BST-2/Tetherin Ectodomain

Andreas Hinz,[1,5] Nolwenn Miguet,[1,5] Ganesh Natrajan,[1] Yoshiko Usami,[2] Hikaru Yamanaka,[2] Patricia Renesto,[1] Bettina Hartlieb,[1] Andrew A. McCarthy,[1,3] Jean-Pierre Simorre,[4] Heinrich Göttlinger,[2] and Winfried Weissenhorn[1,*]
[1]Unit of Virus Host Cell Interactions (UVHCI) UMI 3265 Université Joseph Fourier-EMBL-CNRS, 6 rue Jules Horowitz, 38042 Grenoble, France
[2]Program in Gene Function and Expression, Program in Molecular Medicine, University of Massachusetts Medical School, Worcester, MA 01605, USA
[3]EMBL, 6 rue Jules Horowitz, 38042 Grenoble, France
[4]Institut de Biologie Structurale Jean-Pierre Ebel, UMR 5075 CEA-CNRS-UJF, 41 rue Jules Horowitz, 38027 Grenoble Cedex 01, France
[5]These authors contributed equally to this work
*Correspondence: weissenhorn@embl.fr
DOI 10.1016/j.chom.2010.03.005

SUMMARY

The restriction factor BST-2/tetherin contains two membrane anchors employed to retain some enveloped viruses, including HIV-1 tethered to the plasma membrane in the absence of virus-encoded antagonists. The 2.77 Å crystal structure of the BST-2/tetherin extracellular core presented here reveals a parallel 90 Å long disulfide-linked coiled-coil domain, while the complete extracellular domain forms an extended 170 Å long rod-like structure based on small-angle X-ray scattering data. Mutagenesis analyses indicate that both the coiled coil and the N-terminal region are required for retention of HIV-1, suggesting that the elongated structure can function as a molecular ruler to bridge long distances. The structure reveals substantial irregularities and instabilities throughout the coiled coil, which contribute to its low stability in the absence of disulfide bonds. We propose that the irregular coiled coil provides conformational flexibility, ensuring that BST-2/tetherin anchoring both in the plasma membrane and in the newly formed virus membrane is maintained during virus budding.

INTRODUCTION

Enveloped viruses rely on host cell factors to complete their life cycle. These factors act as positive or negative regulators, such as restriction factors, that often limit replication to a narrow range of hosts and cell types (Malim and Emerman, 2008). While restriction factors are inducible by IFN and thus constitute a first line of innate immune defense, viral proteins that render cells permissive for infection can counteract this mechanism. Certain cell types, such as HeLa cells, require the expression of the HIV-1 cofactor Vpu for particle release (Göttlinger et al., 1993; Klimkait et al., 1990; Strebel et al., 1989; Terwilliger et al., 1989), although replication occurs independently of Vpu in other cells (Gramberg et al., 2009; Strebel et al., 2009). This restriction was attributed to the presence or absence of BST-2, also known as tetherin (or CD317 and HM1.24) (Neil et al., 2008; Van Damme et al., 2008). BST-2/tetherin was originally linked to B cell development and shown to be a marker of multiple myeloma cells (Goto et al., 1994; Masuyama et al., 2009; Ohtomo et al., 1999). Its expression is induced by IFN-α (Kawai et al., 2008), and IFN-α activation leads to HIV-1 retention at the plasma membrane in the absence of Vpu (Neil et al., 2007).

BST-2/tetherin is a type II transmembrane protein composed of a small cytosolic domain, an N-terminal transmembrane region (TMR), and an extracellular domain modified by a second membrane anchor, a C-terminal glycosyl-phosphatidylinositol (GPI) (Kupzig et al., 2003). BST-2/tetherin resides in lipid rafts at the cell surface and membranes of the *trans* Golgi network (TGN) (Kupzig et al., 2003). In HIV-1-infected cells, tetherin is retained in the TGN by Vpu (Neil et al., 2008; Van Damme et al., 2008) and targeted for endocytosis and degradation (Douglas et al., 2009; Goffinet et al., 2009; Harila et al., 2007; Mangeat et al., 2009; Mitchell et al., 2009), although it should be noted that enhancement of virus release by Vpu does not depend on downregulation or degradation of tetherin in some specific cell lines (Miyagi et al., 2009).

Inhibition of tetherin by Vpu is species specific and suggests that Vpu's activity evolved to specifically counteract human tetherin (Goffinet et al., 2009; Gupta et al., 2009; Jia et al., 2009; Sauter et al., 2009). Vpu-mediated tetherin retention requires the TMR of tetherin (McNatt et al., 2009; Rong et al., 2009) or all structural domains (Goffinet et al., 2009) and the TMR and cytosolic domain of Vpu (Van Damme et al., 2008).

The antiviral function of tetherin is not limited to HIV-1 or other retroviruses (Jouvenet et al., 2009; Zhang et al., 2009) as it also restricts release of filoviruses (Jouvenet et al., 2009; Kaletsky et al., 2009), arena viruses (Sakuma et al., 2009a), and KSHV (Bartee et al., 2006) in the absence of their respective antagonists.

Tetherin has been suggested to span both the cellular and viral membranes (Neil et al., 2008) based on its double-membrane-anchored topology (Kupzig et al., 2003), its ability to form disulfide-linked dimers (Ohtomo et al., 1999), and the presence of a predicted coiled-coil sequence in the extracellular domain. Tetherin is present in the viral membrane as a homodimer, and either TMR or the GPI anchor must be inserted into virion

envelopes for successful retention (Perez-Caballero et al., 2009). Furthermore, disulfide crosslinking via any of the three cysteines and the spacer function of the coiled coil are necessary for antiviral activity (Andrew et al., 2009; Perez-Caballero et al., 2009).

Here, we present the crystal structure of a core fragment of human tetherin, which forms a 90 Å long parallel coiled coil. The complete extracellular region adopts a ~170 Å long bent rod-like structure based on small-angle X-ray scattering analysis, defining the extracellular domain as a molecular ruler that keeps both membrane anchors at a certain distance. The coiled coil contains a number of destabilizing residues at central heptad positions, which are conserved among all known tetherin sequences. Consequently, both the core of tetherin and the complete extracellular domain show a dramatic loss in thermostability upon disulfide bond reduction in vitro. Mutagenesis analyses reveal that the coiled coil must be intact for function and identify an N-terminal conserved region that is required for HIV-1 restriction. The structure of tetherin explains how it can bridge long distances using a labile parallel coiled coil. Thus, tetherin has enough flexibility to insert one membrane anchor into a budding virion while the other anchor remains in the plasma membrane and excluded from the site directly involved in budding.

RESULTS

Recombinant Tetherin Forms Dimers

Recombinant tetherin(47-159) elutes from a SEC column at ~10.0 ml (Figure 1A); it migrates at ~13 kDa under reducing and at ~26 kDa under nonreducing conditions on SDS-PAGE, indicating disulfide-linked dimerization (Figure 1B). Since crystals produced from tetherin(47-159) did not diffract beyond 10 Å resolution, we applied limited trypsin proteolysis to define a smaller fragment containing residues 80–147. Tetherin(80-147) elutes from a SEC column at ~11.3 ml (Figure 1A) and reveals disulfide-linked dimerization based on SDS-PAGE analysis under reducing and nonreducing conditions (Figure 1B). In order to test whether dimerization depends mainly on disulfide-mediated crosslinking, both tetherin(47-159) and tetherin(80-147) were reduced with DTT, and cysteines were subsequently blocked with iodoacetamide; this treatment produces mostly monomeric tetherin under nonreducing SDS-PAGE conditions (Figure 1C, lanes 1 and 2). Chemical crosslinking reveals that both constructs still dimerize, as indicated by the appearance of new bands migrating at ~27 kDa (tetherin[47-159]) and between 15 and 20 kDa (tetherin[80-147]) (Figure 1C, lanes 4 and 6). Circular dichroism analyses show a high helical content (~90% helical) for both constructs (Figure 2A). Although the helical content does not change for tetherin(47-159) in the presence of DTT, tetherin(80-147) displays a reduced helical content (~70%) (Figure 2A). The effect of the reducing agent was more dramatic when thermostability was tested. While tetherin(47-159) and tetherin(80-147) show melting temperatures (T_m) of ~61°C and ~57°C, respectively, disulfide bond reduction drops the T_m to ~35°C and ~30°C, respectively (Figure 2B). The influence of disulfide bond linkage on the structure is further corroborated by the increased sensitivity of both constructs to complete degradation by trypsin treatment under reducing conditions (Figure S1). These results indicate that dimer stability greatly depends on intermolecular disulfide bonds.

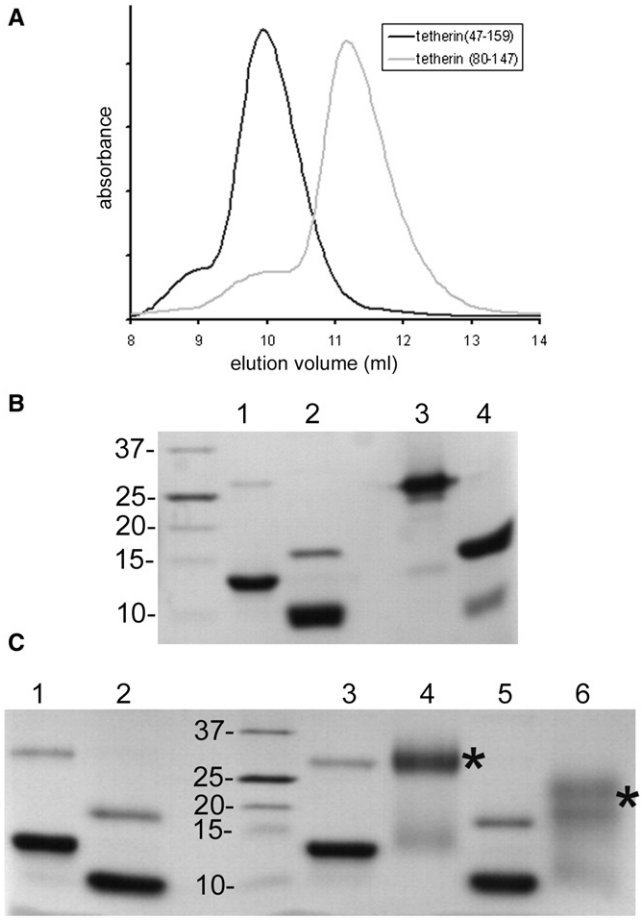

Figure 1. Biochemical Characterization of the Extracellular Domain of Tetherin

(A) SEC analysis of tetherin(47-159) and tetherin(80-147).

(B) SDS-PAGE of tetherin(47-159) (lanes 1 and 3) and tetherin(80-147) under reducing (lanes 1 and 2) and nonreducing conditions (lanes 3 and 4).

(C) Reduced tetherin(47-159) and tetherin(80-147) still dimerize; tetherin (47-159) (lanes 1, 3, 4) and tetherin(80-147) (lanes 2, 5, 6) were treated with iodoacetamide and separated under nonreducing conditions (lanes 1 and 2), under reducing conditions (lanes 3 and 5), and after crosslinking with 5 mM EGS (lanes 4 and 6). Dimers are indicated by *.

Crystal Structure of Tetherin(80-147)

The crystal structure of tetherin(80-147) was determined from a selenomethionine-containing crystal using the single anomalous dispersion (SAD) method and diffraction data to 2.77 Å resolution, which produced a readily interpretable electron density map (Figure 3A). The asymmetric crystal unit contained 11 monomers that, together with crystallographic symmetry, formed six identical dimers. The best-defined dimer contains residues 89–147 and folds into a disulfide-linked 90 Å long parallel coiled coil (Figures 3B). The N-terminal residues 80–88 are disordered, and the coiled coil starts with Cys91 occupying the heptad d position followed by Val95 (a), Leu98 (d), and Leu102 (a). Glu105 (d) and the stutter at Gly109 splay the coiled coil apart, documented by the increase in coiled-coil radius and pitch (Figure S2) beyond the regular coiled-coil features (Phillips, 1992). The heptad positions Val113 (a) and Leu116 (d) still show

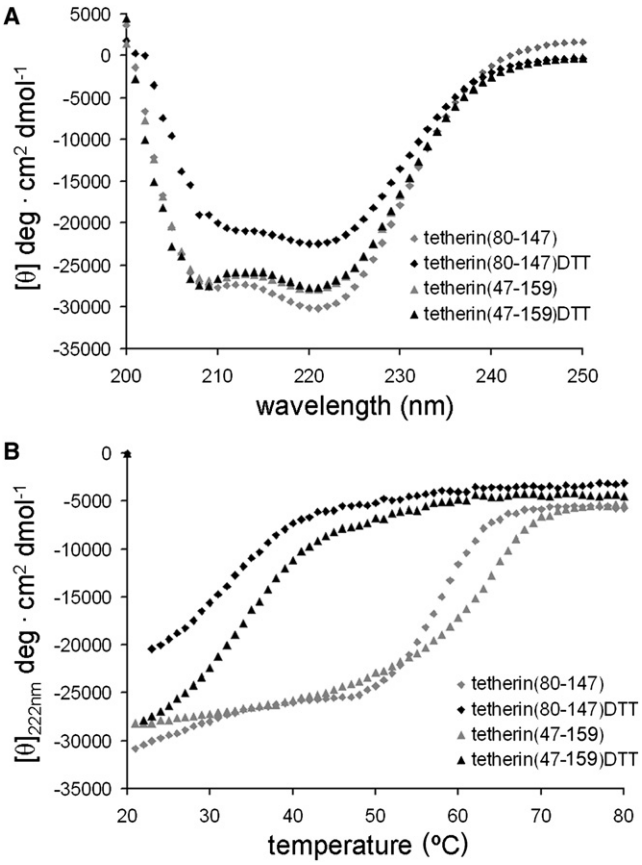

Figure 2. Disulfide Bond Reduction Decreases the Thermostability of Tetherin

(A) Circular dichroism analyses of tetherin under native and reducing conditions (DTT). Disulfide bond reduction of tetherin(80-147) reduces the overall helical content, while tetherin(47-159) is less affected.

(B) Thermostability measurements of tetherin were performed at 222 nm under native and reducing conditions (DTT), revealing a dramatic change in T_m after disulfide bond reduction.

an increased coiled-coil radius and pitch (Figure S2). More regular values are adopted along the heptad positions Ile120 (a), Leu123 (d), and Leu127 (a) (Figure 3C). The irregularities that follow are produced by a stutter at Ala130, which tightens the coiled-coil radius to 4.3 Å (Figure S2), and Asn141 (d), which splays the coiled coil apart (Figures 3C and S2). Despite these irregularities, the coiled coil also contains stabilizing interactions, such as salt bridges (Glu105-Lys106, Glu133-Arg138) and an interhelical hydrogen bond (Asn141) (Figure 3C). All heptad positions are conserved among the known tetherin sequences. Modifications in some sequences include an extra helical turn before Gly100 and/or a deletion of two helical turns determined by Ala130 (a position) and Val134 (d position) (Figure S3).

The N-Terminal Extracellular Region of Tetherin Extends the Rod-like Structure

SEC analysis of tetherin(47-159) shows a larger hydrodynamic radius compared to tetherin(80-149) (Figure 1A). This is further confirmed by small-angle X-ray scattering analysis (Figure 4A). Guinier evaluation reveals radii of gyration (Rg) of 47.5 Å for tetherin(47-159) and 31.9 Å for tetherin(80-149). Maximal protein dimensions (D_{max}) of 170 Å (tetherin[47-159]) and 110 Å (tetherin[80-147]) were calculated by the distance distribution function p(r) (Figure S4). The shapes of the tetherin dimers were determined ab initio, and the reconstructed models fit the experimental data with the discrepancy χ of 1.1 and 1.5, respectively (Figure 4A). The solution structure of tetherin(80-147) shows an elongated rod with dimensions of 110 × 45 × 30 Å, consistent with the 90 Å length of the rod seen in the crystal (Figure 4B). Tetherin(47-159) is more elongated and produces a rod with dimensions of 150 × 60 × 45 Å, confirming that the N-terminal region extends the coiled-coil part (Figure 4C). Part of the N terminus in the rod is slightly bent, and its orientation might be determined by the flexible linkage of the N terminus to the coiled-coil domain, as indicated by the protease sensitivity of this region (Figure S1).

The Coiled Coil and the N-Terminal Region of Tetherin Are Required for HIV-1 Retention

We next analyzed whether disruption of coiled-coil residues influences tetherin function during HIV-1 retention. Two sets of coiled-coil mutations were designed based on the crystal structure; set1 (Cys91Gly, Val95Tyr, Leu98Lys, Leu102His) disrupts the N-terminal part of the coiled coil and set2 (Leu127Lys, Ala130Tyr, Val134Glu, Leu137Glu) disrupts the C-terminal region. Recombinant forms of both mutants, tetherin(47-159)_set1 and tetherin(47-159)_set2, are soluble and elute from a SEC column in peaks overlapping with that of wild-type tetherin(47-159), indicating that the mutations change the hydrodynamic radius of the proteins (Figure S5A). The mutant proteins migrate slightly more slowly on SDS-PAGE than wild-type and reveal reduced disulfide-linked dimerization as determined under nonreducing SDS-PAGE conditions (Figure S5B). Chemical crosslinking corroborates further that the mutations interfere with dimerization; the set1 mutant shows slightly reduced dimer formation, while set2 mutant shows a more dramatic reduction in dimerization as judged by the ratio of monomer dimer bands on SDS-PAGE in comparison to wild-type tetherin(47-159) (Figure S5B). This indicates that disruption of the C-terminal coiled coil leads to a reduced detection of disulfide-linked dimers in vitro, which is most likely due to a defect in dimerization as detected by chemical crosslinking. In contrast, the set1 mutant shows only dramatically reduced disulfide-linked dimerization, although Cys53 and Cys63 are intact and could suffice to form disulfide-linked dimers (Andrew et al., 2009; Perez-Caballero et al., 2009).

Both sets of mutations were introduced into full-length tetherin containing an internal extracellular HA-tag (tetherin[iHA]) for expression in 293T cells. This indicates that tetherin(iHA)_set1 and set2 mutants are expressed on the surface of 293T cells (Figures 5C and 5D); they show membrane staining similar to that of wild-type tetherin (Neil et al., 2008) and tetherin(iHA), which appears to concentrate in patches on the plasma membrane (Figure 5B). However, expression of the full-length tetherin set1 and set2 mutants (C-terminal HA-tag) in cells infected with Vpu-deficient HIV-1 demonstrates that both mutants are no longer able to prevent HIV-1 release, as indicated by the detection of capsid (CA) in the cell culture supernatant at levels similar to the vector control. In contrast, expression of wild-type tetherin completely blocks HIV-1 release, as expected (Figure 6A, left

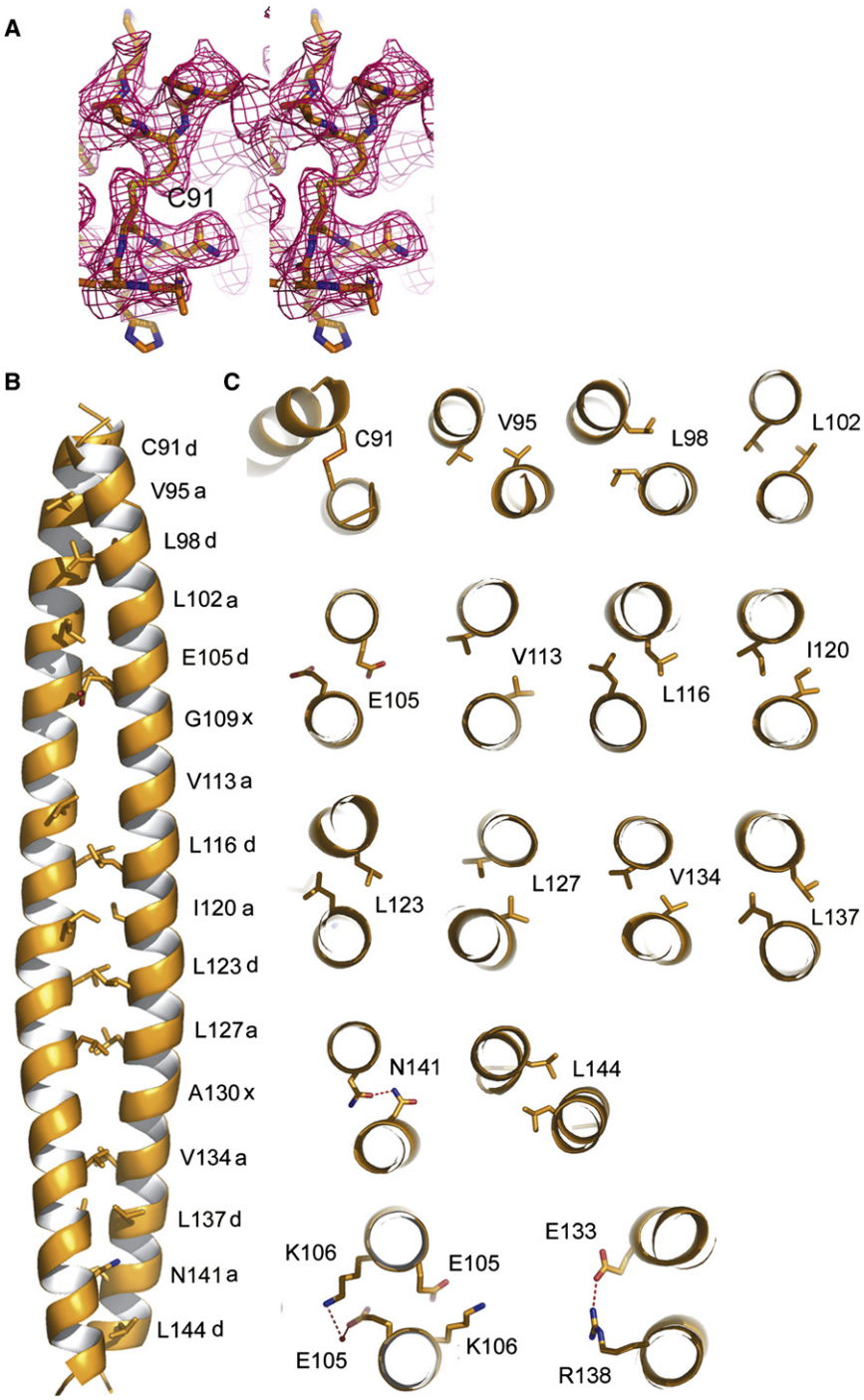

Figure 3. The Crystal Structure of Tetherin(80-147)

(A) Stereo image of the experimental electron density map obtained after SAD phasing and noncrystallographic symmetry averaging; the heptad d position occupied by Cys91 forming a disulfide bond is shown.

(B) Ribbon representation shows a 90 Å parallel coiled coil.

(C) Close-up of the heptad motifs and polar dimerization contacts.

panel). This thus implies that proper coiled-coil formation is required for tetherin function. Both mutants do not affect intracellular processing of Gag and were expressed at similar levels (Figure 6B, middle and right panels).

Since the extracellular region comprising residues 48–71 is highly conserved between different species (Figure S3), we tested two more sets of mutations by replacing conserved charged and polar side chains. Set3 contains changes within residues 47–58 (Lys47Ala, Asn49Gly, Glu51Ala, Arg54Ser, Asp55Ala, Arg58Ser) and set4 within residues 62–73 (Glu62Ala, Arg64Ser, Asn65Ala, His59Ser, Gln71Ala, Gln72Ala, Glu73Ser) (Figure S3). Both mutants are soluble when expressed as tetherin(47-159) and elute from a SEC column at the same position as wild-type tetherin(47-159) (Figure S6A). Furthermore, they form disulfide-linked dimers that can be efficiently crosslinked (Figure S6B). Both mutations were then introduced into full-length tetherin(iHA) and expressed in 293T cells. This demonstrates that both sets (3 and 4) of tetherin(iHA) mutants are expressed at the plasma membrane (Figures 5E and 5F). Although expression of the full-length set3 mutant reveals its activity in HIV-1 retention at a level comparable to wild-type (Figure 6B, left panel, lanes 2 and 3), expression of the set4 mutant shows no retention activity (Figure 6B, left panel, lane 4). Cells from all experiments reveal similar patterns of intracellular Gag processing (Figure 6B, middle panel). However, the extensive posttranslational modification observed for wild-type tetherin expression in 293T cells, which generates a high molecular weight smear, is less characteristic in the case of the set4 mutant (Figure 6B, right panel, lane 4).

Since the set4 mutant includes mutagenesis of the glycosylation site at Asn65, we constructed a single mutant of the glycosylation site at Asn65, Asn65Gln, to test whether the loss of retention activity is due to reduced glycosylation. Although the Asn65Gln mutant shows a less complex expression pattern (Figure 6C, right panel, lane 3), similar to tetherin_set4, the retention of HIV-1 was only slightly affected. A small amount of virus could escape, since CA was detected in the supernatant (Figure 6C, left panel, lane 3). This indicates that the complete loss of retention observed for the set4 mutant is most likely not due to the changes in posttranslational modification. Together, our data indicate that a conserved N-terminal region of the extracellular domain is important for tetherin function.

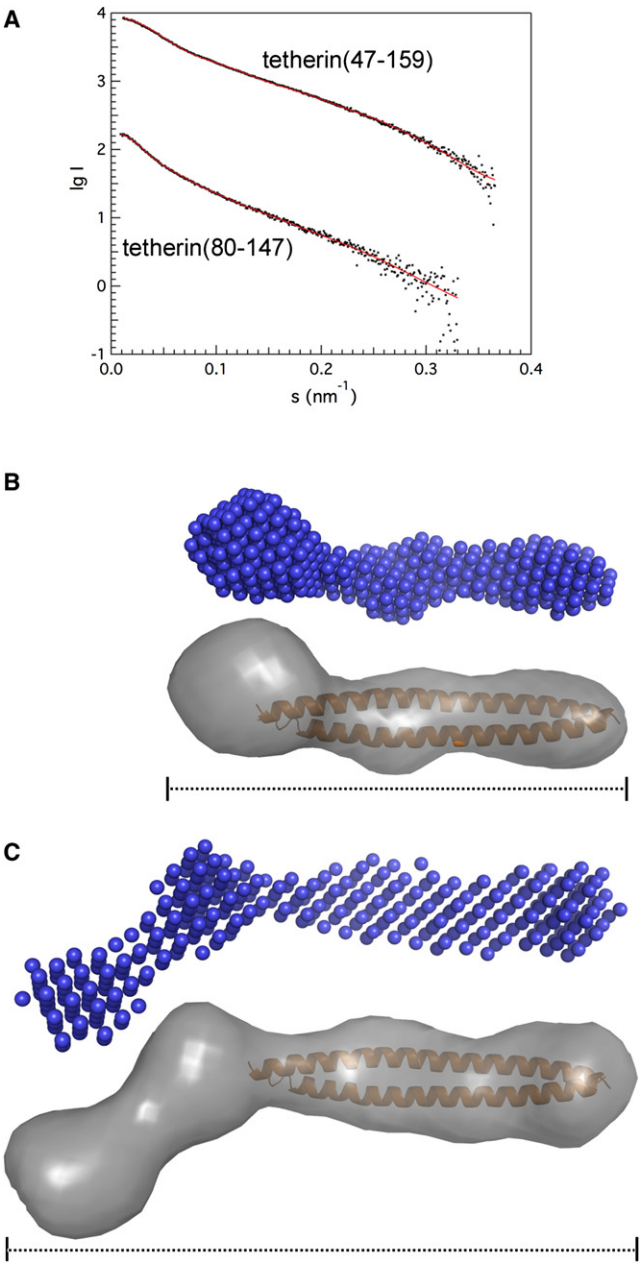

Figure 4. Small-Angle X-Ray Scattering Analysis of Tetherin

(A) Experimental scattering intensities obtained for tetherin(47-159) (upper curve) and tetherin(80-147) (lower curve) are shown as a function of resolution and after averaging and subtraction of solvent scattering. The scattering intensities calculated from representative models (presented in Figures 4B and 4C) with the lowest χ values are shown as red lines. The absolute values of the intensities of the upper curve are shifted by 2 logarithmic units.

(B and C) Ab initio models of tetherin(80-147) (B) and of tetherin(47-159) (C) reveal elongated rod-like structures; the calculated bead model as well as the molecular envelopes with the docked coiled-coil structure are shown.

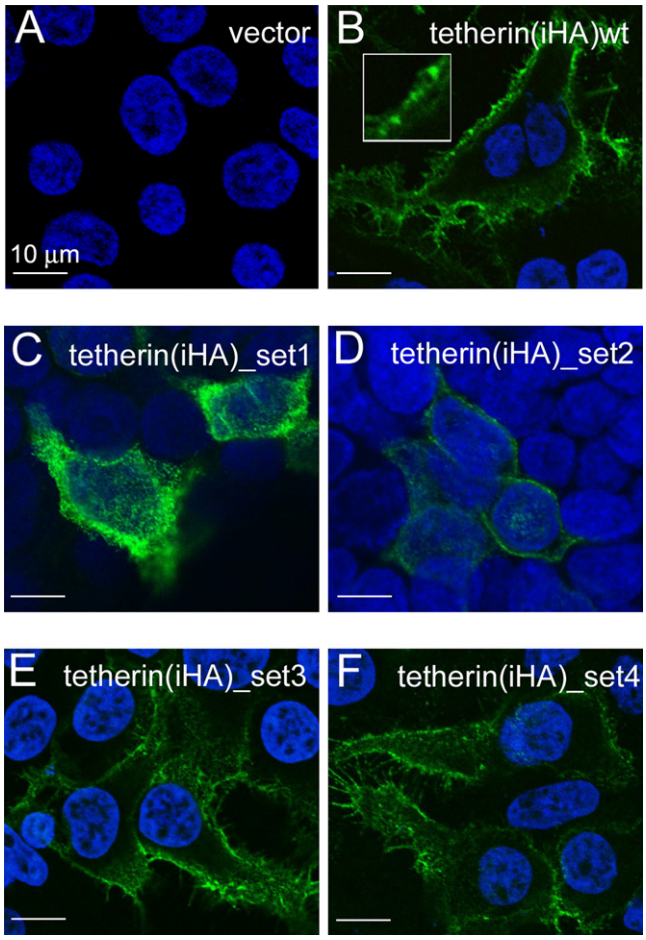

Figure 5. Cellular Localization of Wild-Type Tetherin and Mutant Forms of Tetherin

(A–F) Immunofluorescence of mock-transfected 293T cells showing DAPI staining (A); tetherin(iHA), with the inset showing a close-up of a section of the plasma membrane, revealing patches of tetherin staining (B); tetherin(iHA-set1) (C); tetherin(iHA-set2) (D); tetherin(iHA-set3) (E); and tetherin (iHA-set4) (F). All constructs reveal a similar plasma membrane staining pattern, indicating that the mutations do not affect their localization.

Since the HA-tag of tetherin(iHA) was inserted into a flexible region (Figure S3) that is disordered in the crystal structure and sensitive to proteolysis (Figure S1), we tested the effect of the insertion on tetherin function. Expression of tetherin(iHA) reveals a slightly reduced HIV-1 retention activity in comparison to wild-type tetherin, as judged by the detection of CA in the supernatant (Figure 6D, left panel, lanes 2 and 3). Both wild-type and tetherin(iHA) show similar expression patterns (Figure 6D, right panel) and accumulation of intracellular Gag as compared to the vector control (Figure 6D, middle panel). This indicates that the conformational flexibility within residues 80–88 tolerates the insertion of the HA-tag but slightly reduces the efficacy of HIV-1 retention. Although we lack high-resolution structural information of the N terminus, the flexible region accommodating the HA-tag might correspond to the bent conformation of tetherin(47-159) observed in the model calculated based on SAXS data (Figure 4C).

DISCUSSION

Tetherin inhibits the release of some enveloped viruses, including HIV-1, in the absence of Vpu (Neil et al., 2008) by

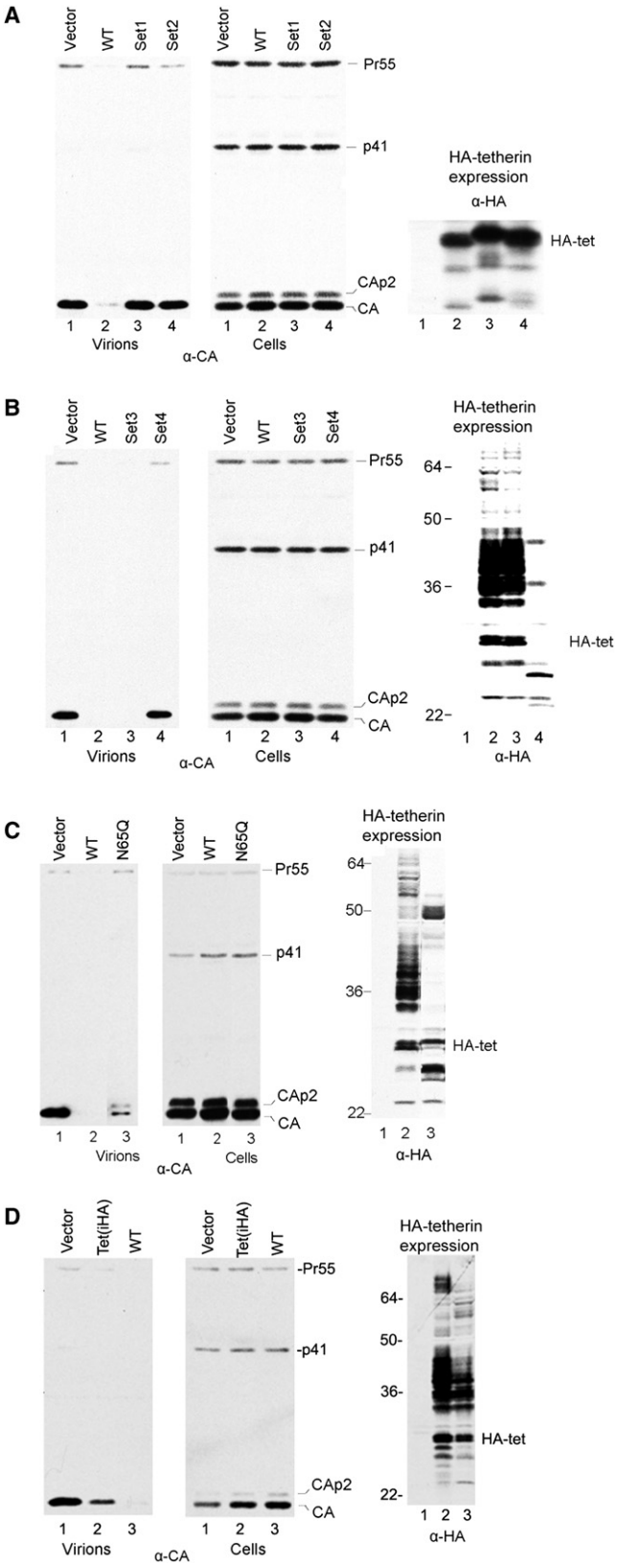

Figure 6. Mutations within the Coiled Coil and the N-Terminal Region Affect Tetherin Function during HIV-1 Retention

(A) Expression of tetherin_set1 and tetherin_set2 abolishes the retention function of tetherin. Release of virions (left panel, lanes 3 and 4) is the same as in case of the vector control (lane 1), whereas wild-type tetherin prevents virion release (left panel, lane 2). The middle panel shows that intracellular Gag and its processing are not affected by the expression of mutant tetherin (lanes 3 and 4). The right panel shows the expression levels of mutant (lanes 3 and 4) and wild-type tetherin (lane 2).

(B) Expression of tetherin_set3 (left panel) has no effect on tetherin function (lane 3) while tetherin_set4 abolishes the retention function of tetherin (lane 4), as indicated by the extracellular detection of CA. The middle panel shows that intracellular Gag and its processing are not affected by the expression of mutant tetherin (lanes 3 and 4). The right panel shows the expression levels of mutant and wild-type tetherin. Note that the extensive posttranslational modification observed for wild-type tetherin is absent in case of the set4 mutant.

(C) Expression of the tetherin mutant Asn65Gln (N65Q) (left panel) has little effect on tetherin function (lane 3) compared to wild-type tetherin (lane 2). Intracellular Gag processing is not affected by the expression of the N65Q mutant (middle panel, lanes 2 and 3). The right panel shows that the expression pattern of N65Q (lane 3) is less complex than that of wild-type tetherin (lane 2).

(D) Expression of tetherin(iHA) (left panel) has little effect on tetherin function (lane 2) when compared to wild-type tetherin (lane 3). The middle panel shows that intracellular Gag and its processing are not affected. The right panel shows the expression levels of tetherin(iHA) and wild-type tetherin.

bridging cellular and viral membranes (Perez-Caballero et al., 2009) (Fitzpatrick et al., 2010). Our structural analyses demonstrate that the complete extracellular domain of tetherin adopts an extended conformation that spans a maximal distance of 170 Å. More than half of this is provided by a 90 Å long parallel coiled coil. The low-resolution model based on X-ray scattering data indicates a slightly bent orientation of the N-terminal domain with respect to the coiled coil. This might be due to flexibility within the region (residues 79–89) connecting the N-terminal and coiled-coil domains, as documented by the sensitivity to proteolysis and the absence of an ordered structure for residues 80–88. In addition, this region permits the insertion of a HA-tag epitope without substantial loss of tetherin function.

The extracellular rod-like structure must be connected to the TMR via three N-terminal residues and to the GPI anchor via one C-terminal residue. Consequently, it is unlikely that tetherin is positioned parallel between cellular and viral membranes, which would tether virions quite close to the plasma membrane. The distance between both membranes would be less than 3–5 nm. Thin-section electron microscopy images support a larger distance between virions and the plasma membrane (Neil et al., 2008; Perez-Caballero et al., 2009). Thus, upon virion tethering, the dimeric tetherin rod has most likely one end anchored in the plasma membrane and the other one in the virus membrane, as hypothesized (Perez-Caballero et al., 2009).

The length of the rod and its rather rigid structure in solution suggest that it functions as a molecular ruler that connects two entities via a 170 Å distance. The importance of the spacer function is documented by our mutagenesis studies of the coiled-coil region and by the deletion of the coiled coil (Perez-Caballero et al., 2009), both of which lead to a loss of the HIV-1 retention function. Such a molecular ruler function might be also required to connect adjacent lipid rafts within the plasma membrane (Kupzig et al., 2003).

Single cysteine mutations do not affect tetherin function dramatically, but mutagenesis of all three cysteines led to a complete loss of function during HIV-1 release (Andrew et al., 2009; Perez-Caballero et al., 2009), although the mutant is still active during Lassa and Marburg virus VLP release (Sakuma et al., 2009b). We show that the presence of disulfide bonds is crucial for the stability of the extracellular domain, since the T_m drops to 35°C (tetherin[47-159]) under reducing conditions. The low stability of tetherin under reducing conditions is most likely due to instability of the coiled coil, which shows an even lower T_m under reducing conditions. The coiled coil contains a number of coiled-coil-destabilizing residues occupying central heptad positions. These positions do not follow classical knobs-into-holes packing but instead loosen the coiled-coil pitch and induce an expansion of its radius. Although the coiled-coil region contains two interhelical salt bridges and one interhelical hydrogen bond, which are employed to stabilize coiled coils (Burkhard et al., 2002), the solvent exposure of the apolar heptad positions (Li et al., 2003) might contribute to the dramatic instability of the coiled coil in the absence of the disulfide bond. Together, these structural features explain the low T_m in the absence of stabilizing disulfide bonds.

This mode of labile coiled-coil interactions might serve two functions. First, tetherin's cellular function might involve the formation of heterodimers with a yet unknown ligand employing its coiled coil to form more stable dimers. Second, the weak coiled-coil interactions together with the stabilizing disulfide bonds generate a dynamic structure, which permits disassembly and reassembly of the coiled coil during dynamic processes. The latter function is in agreement with the presence of similar dynamic or destabilizing coiled-coil features in myosin (Blankenfeldt et al., 2006; Li et al., 2003), tropomyosin (Brown et al., 2001), and the streptococcus M1 protein (McNamara et al., 2008) that have been suggested to be important for their mode of action.

Despite its instability in vitro, we demonstrate the importance of the coiled coil in vivo. Mutagenesis of N- and C-terminal sets of highly conserved heptad positions eliminates the tethering function, although the mutant proteins are still expressed on the plasma membrane. This indicates that the spacer function provided by proper coiled-coil formation is essential for tethering. We also identified a third set of residues within the highly conserved N-terminal extracellular region that are functionally required. Mutations within the stretch of residues 48–59 have no effect on tethering, whereas changes within residues 62–73 lead to a loss of the tethering function. Again, both mutant proteins are expressed on the plasma membrane, and the extracellular domains form dimers in vitro. Since the set4 mutant eliminates the glycosylation site at Asn65 and shows a less complex expression pattern than wild-type tetherin, we tested whether changes in posttranslational modification are responsible for loss of tetherin function. Although the expression pattern of Asn65Gln resembles that of the set4 mutant, it shows only slightly reduced HIV-1 retention activity, consistent with previous findings reporting no effect on HIV-1 retention of single and double glycosylation mutants of tetherin (Andrew et al., 2009). This indicates that mutagenesis of this N-terminal region (set4) either affects its spacer function or eliminates an important docking site, possibly for self-assembly. Although Perez-Caballero et al. reported that the N terminus can be replaced by a similar region derived from the transferrin receptor and the coiled coil can be replaced by the dystrophia myotonica protein kinase coiled coil, it is important to note that the activity of art-tetherin is ~10-fold lower (Perez-Caballero et al., 2009). In contrast, our data clearly demonstrate that the N-terminal domain and the dynamic features of the coiled coil of tetherin are essential for HIV-1 retention.

Based on our structural analysis, we propose the following interplay between the elongated shape and the conformational flexibility of tetherin. Although we do not know at which stage of assembly tetherin enters the virion membrane, it is likely that it is present from the beginning of assembly starting from lipid rafts. Since virus assembly and budding is a dynamic process, tetherin cannot remain too rigid. The coiled-coil instabilities thus permit a certain degree of flexibility for the tetherin dimers to diffuse laterally into the budding site with four membrane anchors while maintaining the strict distance between the membrane anchors. The conformational flexibility, which entails most likely opening and reassembly of the coiled coil, is facilitated by the presence of the disulfide bonds. Consequently, dimer dissociation and restabilization do not interfere with the dynamic process of virus assembly and budding, and tetherin remains anchored in the newly formed viral membrane, maintaining its spacer function. Furthermore, the elongated rod-like structure might be involved in self-assembly, as supported by the punctate appearance of tetherin in the plasma membrane. Such clustering might require an intact N-terminal region, which could cluster tetherin around the membrane neck of a budding virion, consistent with the accumulation of tetherin at HIV-1 budding sites (Habermann et al., 2010). This would ensure that at least one or several tetherin dimers can efficiently insert into the viral membrane to render the system efficient. Finally, the structural basis, which controls tetherin incorporation into virions even in the presence of Vpu in some cells without restriction of HIV-1 release (Fitzpatrick et al., 2010), may depend on its surface density (Habermann et al., 2010) but remains to be determined.

EXPERIMENTAL PROCEDURES

Bacterial Protein Expression and Purification

cDNA encoding human tetherin/BST-2 residues 47–159 and 80–147 was cloned into expression vector pETM11. Site-directed mutagenesis of tetherin (47-159) was carried out using standard protocols and verified by sequencing. Protein expression was performed in *E. coli* Rosetta2 cells induced with isopropyl β-D-1-thiogalactopyranoside (IPTG) at 20°C for 4 hr. Cells were lysed in buffer A (20 mM Tris [pH 8.0], 0.1 M NaCl, 10 mM imidazole), and proteins were purified by Ni^{2+} chromatography. The His-tag was removed by tobacco etch virus (TEV) protease cleavage, and both TEV and uncleaved protein were removed by Ni^{2+} chromatography. Final purification steps included anion-exchange chromatography (mono Q; GE Healthcare; Waukesha, WI) in buffer B (20 mM bicine [pH 9.3], 0.1 M NaCl, 5 mM EDTA) and size-exclusion chromatography (Superdex 75; GE Healthcare) in buffer C (20 mM HEPES [pH 8.0], 0.1 M NaCl, 5 mM EDTA). Selenomethionine-substituted tetherin(80-147) and mutant tetherin proteins were purified as described above. Mutant tetherin constructs contain the following mutations: tetherin_set1, Cys91Gly, Val95Tyr, Leu98Lys, Leu102His; tetherin_set2, Leu127Lys, Ala130Tyr, Val134Glu, Leu137Glu; tetherin_set3, Lys47Ala, Asn49Gly, Glu51Ala, Arg54Ser, Asp55Ala, Arg58Ser; tetherin_set4, Glu62Ala, Arg64Ser, Asn65Ala, His59Ser, Gln71Ala, Gln72Ala, Glu73Ser.

Crystallization, Data Collection, and Structure Solution

Tetherin(80-147) was crystallized at a concentration of 5 mg/ml by mixing 1 μl protein and 1 μl reservoir solution (0.02 M $MgCl_2$, 0.1 M bis tris [pH 5.0], 20%

polyacrylic acid) at 20°C. Crystals were cryoprotected in reservoir solution supplemented by 26% glycerol and flash-frozen in liquid nitrogen. A SAD data set was collected at ESRF (Grenoble, France), beamline ID14-4. Data were indexed and processed with XDS (Kabsch, 1993) and scaled with SCALA (CCP4, 1994; Evans, 2006). The crystals belong to space group C2 with unit cell dimensions of a = 169.89Å, b = 85.93Å, c = 123.31Å, and β = 126.94° and contain 11 monomers per asymmetric unit.

Heavy-atom positions were located with SHELXD (Schneider and Sheldrick, 2002), and the correct hand was verified using SHELXE (Sheldrick, 2002). The experimental phases were calculated using SHARP (Bricogne et al., 2003) and resulted in an overall figure of merit (FOM) of 0.38/0.10 for the acentric and centric reflections, respectively. These phases were improved using a 70% solvent content in SOLOMON (Abrahams and Leslie, 1996). An initial model was built using RESOLVE (Terwilliger and Berendzen, 1999), which allowed the determination of the noncrystallographic symmetry operators. The electron density map was further improved using 11-fold averaging, and the final model was built manually using the program COOT (Emsley and Cowtan, 2004). The structure was refined to a resolution of 2.77 Å with the program PHENIX (Adams et al., 2002), with an R_{factor} of 0.24 and R_{free} of 0.27 with good stereochemistry (Table 1). Most (96.88%) of the residues are within the preferred and allowed regions of a Ramachandran plot (CCP4, 1994). Chains A, F, I, and J contain amino acids (aa) 89–147; chain B, aa 89–145; chain C, aa 89–137; chain D, aa 87–142; chain E, aa 88–146; chain G, aa 88–141; chain H, aa 89–142; and chain K, aa 89–127. Molecular graphics figures were generated with PyMOL (http://www.pymol.org). The helical parameters of the coiled coil were calculated using the program TWISTER (Strelkov and Burkhard, 2002).

Table 1. Crystallographic Statistics

Data Collection Statistics	
Space group	C2
Cell dimensions a, b, c; β	169.89 Å, 85.93 Å, 123.31 Å; 126.94°
Wavelength (Å)	0.979
Resolution (Å)	45.00–2.77 (2.92–2.77)
R_{merge}	0.086 (0.479)
Completeness (%)	98.1 (97.7)
I/σ(I)	13.8 (3.8)
Redundancy	7.6 (7.7)
Refinement Statistics	
Resolution range (Å)	44.8–2.77
No. reflections	35,361
R_{work}/R_{free}	0.2407/0.2737
No. protein atoms	4596
No. of ligands/ion	21
No. of waters	126
B factors protein/ligand/water	88.56/62.65/66.31
Rmsd (bonds) (Å)	0.014
Rmsd (angles) (°)	1.305

Values in parentheses are for highest-resolution shell.

Biophysical and Biochemical Characterization of Tetherin

CD spectroscopy measurements were performed using a JASCO Inc. (Easton, MD) spectropolarimeter equipped with a thermoelectric temperature controller. Spectra of each sample were recorded at 20°C in buffer D (20 mM phosphate [pH 7], 100 mM NaCl). For thermal denaturation experiments, the ellipticity was recorded at 222 nm with 1°C steps from 20°C to 100°C, with a slope of 1°C/min. Ellipticity values were converted to mean residue ellipticity.

Proteolysis of tetherin was carried out in buffer C at room temperature (RT) with a trypsin-to-protein ratio of 1:100 (w/w). Dimerization of tetherin under reducing conditions was tested as follows: Proteins were reduced with 10 mM DTT and subsequently incubated with 100 mM iodoacetamide at RT for 1 hr. Unbound DTT and iodoacetamide were removed by dialysis in buffer C, and samples were crosslinked with 5 mM ethylene glycol bis(succinimidyl succinate) (EGS). The crosslinking reaction was quenched with 20 mM Tris (pH 8.0).

Small-Angle X-Ray Scattering Analysis

X-ray scattering data were collected on ESRF (Grenoble) beamline ID14-EH3 at a sample-detector distance of 2.4 m covering a range of momentum transfer of $0.1 < s < 4.5$ nm^{-1} ($s = 4\pi \sin(\theta)/\lambda$, where θ is the scattering angle and λ = 0.15 nm is the X-ray wavelength). The scattering intensity of tetherin(47-159) was measured at protein concentrations of 2 and 13 mg/ml and that of tetherin(80-147) at concentrations of 2 and 11 mg/ml in buffer C. The data were normalized to the intensity of the incident beam; the scattering of the buffer was subtracted and the resulting intensities were scaled for concentration. Data processing was performed using the program package PRIMUS (Konarev et al., 2003). The forward scattering, *I(0)*, and the Rg were calculated with GNOM, which also provides the distance distribution function, *p(r)*, of the particle (Svergun, 1992). Low-resolution models of both tetherin samples were simulated by the program DAMMIN (Svergun, 1999) and GASBOR (Svergun et al., 2001), which resulted in similar elongated structures. Figure 4 represents the GASBOR model. The crystal structure of tetherin(80-147) was docked into the low-resolution models using the program package SITUS (Wriggers et al., 1999).

Mammalian Expression Constructs and HIV-1 Release Assay

The coding sequence for full-length human tetherin with an N-terminal HA-tag (HA-tetherin) or an HA-tag inserted into the extracellular domain between residues Gln82 and Asp83 (tetherin[iHA]) was cloned into the mammalian expression vector pBJ5. To examine the effects of WT and mutant tetherin on HIV-1 release, 293T cells (1.2×10^6) were seeded into T25 flasks and transfected 24 hr later using a calcium phosphate precipitation technique. The cultures were transfected with 1 μg Vpu-negative proviral DNA ($HIV\text{-}1_{HXB2}$) together with expression vectors for WT or mutant HA-tetherin or the empty vector (50 ng). The total amount of transfected DNA was brought to 8 μg with carrier DNA (pTZ18U). Twenty-four hours posttransfection, the cells were lysed in radioimmunoprecipitation assay buffer (140 mM NaCl, 8 mM Na_2HPO_4, 2 mM NaH_2PO_4, 1% NP-40, 0.5% sodium deoxycholate, 0.05% SDS), and the culture supernatants were clarified by low-speed centrifugation and passed through 0.45 μm filters. Virions released into the medium were pelleted through 20% sucrose cushions by ultracentrifugation for 2 hr at 27,000 rpm and 4°C in a Beckman SW41 rotor. Pelletable material and the cell lysates were analyzed by SDS-PAGE and western blotting, using the anti-HIV CA antibody 183-H12-5C (Chesebro et al., 1992) to detect Gag proteins. HA-tagged tetherin was detected with the anti-HA mouse monoclonal antibody HA.11.

Immunofluorescence Analysis

Tetherin expression vectors containing the extracellular internal HA-tag were transfected into 293T cells using standard methods. For indirect immunofluorescence (IIF), 293T cells were cultured on coverslips and fixed with 4% paraformaldehyde for 20 min at 4°C. The coverslips were incubated with an αHA-tag antibody in PBS for 1 hr at RT. Slides were washed three times with PBS, followed by the secondary antibody incubation at RT for 1 hr (Alexa 488- or 594-coupled anti-mouse or anti-rabbit goat antibodies in PBS). After three washes with PBS, slides were mounted in Mowiol and analyzed by confocal microscopy.

ACCESSION NUMBERS

Coordinates and structure factors have been deposited in the Protein Data Bank with accession number 2x7a.

SUPPLEMENTAL INFORMATION

Supplemental Information includes six figures and can be found with this article online at doi:10.1016/j.chom.2010.03.005.

ACKNOWLEDGMENTS

This work was supported by the Agence Nationale de la Recherche (ANR-08-BLAN-0271-01 to W.W.), the Deutsche Forschungsgemeinschaft (DFG SPP1175 to W.W.), the National Institute of Allergy and Infectious Diseases (R37AI029873 to H.G.), and a postdoctoral fellowship from the European Molecular Biology Organization (B.H.). We thank S. Avilov for help with confocal microscopy and B. Connell for characterization of the first tetherin constructs. We acknowledge the Partnership for Structural Biology (http://www.psb-grenoble.eu) for access to the common platforms, including the crystallization facility (J. Marquez), and the ESRF and EMBL for beam time and assistance during data collection. The following reagent was obtained through the AIDS Research and Reference Reagent Program, Division of AIDS, NIAID, NIH: HIV-1 p24 monoclonal antibody (183-H12-5C) from Bruce Chesebro and Kathy Wehrly.

Received: December 18, 2009
Revised: February 11, 2010
Accepted: March 8, 2010
Published online: April 15, 2010

REFERENCES

Abrahams, J.P., and Leslie, A.G. (1996). Methods used in the structure determination of bovine mitochondrial F1 ATPase. Acta Crystallogr. D Biol. Crystallogr. *52*, 30–42.

Adams, P.D., Grosse-Kunstleve, R.W., Hung, L.-W., Ioerger, T.R., McCoy, A.J., Moriarty, N.W., Read, R.J., Sacchettini, J.C., Sauter, N.K., and Terwilliger, T.C. (2002). PHENIX: building new software for automated crystallographic structure determination. Acta Crystallogr. D Biol. Crystallogr. *58*, 1948–1954.

Andrew, A.J., Miyagi, E., Kao, S., and Strebel, K. (2009). The formation of cysteine-linked dimers of BST-2/tetherin is important for inhibition of HIV-1 virus release but not for sensitivity to Vpu. Retrovirology *6*, 80.

Bartee, E., McCormack, A., and Früh, K. (2006). Quantitative membrane proteomics reveals new cellular targets of viral immune modulators. PLoS Pathog. *2*, e107.

Blankenfeldt, W., Thomä, N.H., Wray, J.S., Gautel, M., and Schlichting, I. (2006). Crystal structures of human cardiac beta-myosin II S2-Delta provide insight into the functional role of the S2 subfragment. Proc. Natl. Acad. Sci. USA *103*, 17713–17717.

Bricogne, G., Vonrhein, C., Flensburg, C., Schiltz, M., and Paciorek, W. (2003). Generation, representation and flow of phase information in structure determination: recent developments in and around SHARP 2.0. Acta Crystallogr. D Biol. Crystallogr. *59*, 2023–2030.

Brown, J.H., Kim, K.H., Jun, G., Greenfield, N.J., Dominguez, R., Volkmann, N., Hitchcock-DeGregori, S.E., and Cohen, C. (2001). Deciphering the design of the tropomyosin molecule. Proc. Natl. Acad. Sci. USA *98*, 8496–8501.

Burkhard, P., Ivaninskii, S., and Lustig, A. (2002). Improving coiled coil stability by optimizing ionic interactions. J. Mol. Biol. *318*, 901–910.

CCP4 (Collaborative Computational Project, Number 4) (1994). The CCP4 suite: programs for protein crystallography. Acta Crystallogr. D Biol. Crystallogr. *50*, 760–763.

Chesebro, B., Wehrly, K., Nishio, J., and Perryman, S. (1992). Macrophage-tropic human immunodeficiency virus isolates from different patients exhibit unusual V3 envelope sequence homogeneity in comparison with T-cell-tropic isolates: definition of critical amino acids involved in cell tropism. J. Virol. *66*, 6547–6554.

Douglas, J.L., Viswanathan, K., McCarroll, M.N., Gustin, J.K., Früh, K., and Moses, A.V. (2009). Vpu directs the degradation of the human immunodeficiency virus restriction factor BST-2/Tetherin via a betaTrCP-dependent mechanism. J. Virol. *83*, 7931–7947.

Emsley, P., and Cowtan, K. (2004). Coot: model-building tools for molecular graphics. Acta Crystallogr. D Biol. Crystallogr. *60*, 2126–2132.

Evans, P. (2006). Scaling and assessment of data quality. Acta Crystallogr. D Biol. Crystallogr. *62*, 72–82.

Fitzpatrick, K., Skasko, M., Deerinck, T.J., Crum, J., Ellisman, M.H., and Guatelli, J. (2010). Direct restriction of virus release and incorporation of the interferon-induced protein BST-2 into HIV-1 particles. PLoS Pathog. *6*, e1000701.

Goffinet, C., Allespach, I., Homann, S., Tervo, H.M., Habermann, A., Rupp, D., Oberbremer, L., Kern, C., Tibroni, N., Welsch, S., et al. (2009). HIV-1 antagonism of CD317 is species specific and involves Vpu-mediated proteasomal degradation of the restriction factor. Cell Host Microbe *5*, 285–297.

Goto, T., Kennel, S.J., Abe, M., Takishita, M., Kosaka, M., Solomon, A., and Saito, S. (1994). A novel membrane antigen selectively expressed on terminally differentiated human B cells. Blood *84*, 1922–1930.

Göttlinger, H.G., Dorfman, T., Cohen, E.A., and Haseltine, W.A. (1993). Vpu protein of human immunodeficiency virus type 1 enhances the release of capsids produced by gag gene constructs of widely divergent retroviruses. Proc. Natl. Acad. Sci. USA *90*, 7381–7385.

Gramberg, T., Sunseri, N., and Landau, N.R. (2009). Accessories to the crime: recent advances in HIV accessory protein biology. Curr. HIV/AIDS Rep. *6*, 36–42.

Gupta, R.K., Hué, S., Schaller, T., Verschoor, E., Pillay, D., and Towers, G.J. (2009). Mutation of a single residue renders human tetherin resistant to HIV-1 Vpu-mediated depletion. PLoS Pathog. *5*, e1000443.

Habermann, A., Krijnse Locker, J., Oberwinkler, H., Eckhardt, M., Homann, S., Andrew, A., Strebel, K., and Kräusslich, H.-G. (2010). CD317/Tetherin is enriched in the HIV-1 envelope 1 and downregulated from the plasma membrane upon virus infection. J. Virol., in press. Published online February 10, 2010. 10.1128/JVI.02421-09.

Harila, K., Salminen, A., Prior, I., Hinkula, J., and Suomalainen, M. (2007). The Vpu-regulated endocytosis of HIV-1 Gag is clathrin-independent. Virology *369*, 299–308.

Jia, B., Serra-Moreno, R., Neidermyer, W., Rahmberg, A., Mackey, J., Fofana, I.B., Johnson, W.E., Westmoreland, S., and Evans, D.T. (2009). Species-specific activity of SIV Nef and HIV-1 Vpu in overcoming restriction by tetherin/BST2. PLoS Pathog. *5*, e1000429.

Jouvenet, N., Neil, S.J., Zhadina, M., Zang, T., Kratovac, Z., Lee, Y., McNatt, M., Hatziioannou, T., and Bieniasz, P.D. (2009). Broad-spectrum inhibition of retroviral and filoviral particle release by tetherin. J. Virol. *83*, 1837–1844.

Kabsch, W. (1993). Automatic processing of rotation diffraction data from crystals of initially unknown symmetry and cell constants. J. Appl. Cryst. *26*, 795–800.

Kaletsky, R.L., Francica, J.R., Agrawal-Gamse, C., and Bates, P. (2009). Tetherin-mediated restriction of filovirus budding is antagonized by the Ebola glycoprotein. Proc. Natl. Acad. Sci. USA *106*, 2886–2891.

Kawai, S., Azuma, Y., Fujii, E., Furugaki, K., Ozaki, S., Matsumoto, T., Kosaka, M., and Yamada-Okabe, H. (2008). Interferon-alpha enhances CD317 expression and the antitumor activity of anti-CD317 monoclonal antibody in renal cell carcinoma xenograft models. Cancer Sci. *99*, 2461–2466.

Klimkait, T., Strebel, K., Hoggan, M.D., Martin, M.A., and Orenstein, J.M. (1990). The human immunodeficiency virus type 1-specific protein vpu is required for efficient virus maturation and release. J. Virol. *64*, 621–629.

Konarev, P.V., Volkov, V.V., Sokolova, A.V., Koch, M.H.J., and Svergun, D.I. (2003). PRIMUS: a Windows PC-based system for small-angle scattering data analysis. J. Appl. Cryst. *36*, 1277–1282.

Kupzig, S., Korolchuk, V., Rollason, R., Sugden, A., Wilde, A., and Banting, G. (2003). Bst-2/HM1.24 is a raft-associated apical membrane protein with an unusual topology. Traffic *4*, 694–709.

Li, Y., Brown, J.H., Reshetnikova, L., Blazsek, A., Farkas, L., Nyitray, L., and Cohen, C. (2003). Visualization of an unstable coiled coil from the scallop myosin rod. Nature *424*, 341–345.

Malim, M.H., and Emerman, M. (2008). HIV-1 accessory proteins—ensuring viral survival in a hostile environment. Cell Host Microbe *3*, 388–398.

Mangeat, B., Gers-Huber, G., Lehmann, M., Zufferey, M., Luban, J., and Piguet, V. (2009). HIV-1 Vpu neutralizes the antiviral factor Tetherin/BST-2

by binding it and directing its beta-TrCP2-dependent degradation. PLoS Pathog. *5*, e1000574.

Masuyama, N., Kuronita, T., Tanaka, R., Muto, T., Hirota, Y., Takigawa, A., Fujita, H., Aso, Y., Amano, J., and Tanaka, Y. (2009). HM1.24 is internalized from lipid rafts by clathrin-mediated endocytosis through interaction with alpha-adaptin. J. Biol. Chem. *284*, 15927–15941.

McNamara, C., Zinkernagel, A.S., Macheboeuf, P., Cunningham, M.W., Nizet, V., and Ghosh, P. (2008). Coiled coil irregularities and instabilities in group A Streptococcus M1 are required for virulence. Science *319*, 1405–1408.

McNatt, M.W., Zang, T., Hatziioannou, T., Bartlett, M., Fofana, I.B., Johnson, W.E., Neil, S.J., and Bieniasz, P.D. (2009). Species-specific activity of HIV-1 Vpu and positive selection of tetherin transmembrane domain variants. PLoS Pathog. *5*, e1000300.

Mitchell, R.S., Katsura, C., Skasko, M.A., Fitzpatrick, K., Lau, D., Ruiz, A., Stephens, E.B., Margottin-Goguet, F., Benarous, R., and Guatelli, J.C. (2009). Vpu antagonizes BST-2-mediated restriction of HIV-1 release via beta-TrCP and endo-lysosomal trafficking. PLoS Pathog. *5*, e1000450.

Miyagi, E., Andrew, A.J., Kao, S., and Strebel, K. (2009). Vpu enhances HIV-1 virus release in the absence of Bst-2 cell surface down-modulation and intracellular depletion. Proc. Natl. Acad. Sci. USA *106*, 2868–2873.

Neil, S.J., Sandrin, V., Sundquist, W.I., and Bieniasz, P.D. (2007). An interferon-alpha-induced tethering mechanism inhibits HIV-1 and Ebola virus particle release but is counteracted by the HIV-1 Vpu protein. Cell Host Microbe *2*, 193–203.

Neil, S.J., Zang, T., and Bieniasz, P.D. (2008). Tetherin inhibits retrovirus release and is antagonized by HIV-1 Vpu. Nature *451*, 425–430.

Ohtomo, T., Sugamata, Y., Ozaki, Y., Ono, K., Yoshimura, Y., Kawai, S., Koishihara, Y., Ozaki, S., Kosaka, M., Hirano, T., and Tsuchiya, M. (1999). Molecular cloning and characterization of a surface antigen preferentially overexpressed on multiple myeloma cells. Biochem. Biophys. Res. Commun. *258*, 583–591.

Perez-Caballero, D., Zang, T., Ebrahimi, A., McNatt, M.W., Gregory, D.A., Johnson, M.C., and Bieniasz, P.D. (2009). Tetherin inhibits HIV-1 release by directly tethering virions to cells. Cell *139*, 499–511.

Phillips, G.N., Jr. (1992). What is the pitch of the α-helical coiled coil? Proteins *14*, 425–429.

Rong, L., Zhang, J., Lu, J., Pan, Q., Lorgeoux, R.P., Aloysius, C., Guo, F., Liu, S.L., Wainberg, M.A., and Liang, C. (2009). The transmembrane domain of BST-2 determines its sensitivity to down-modulation by human immunodeficiency virus type 1 Vpu. J. Virol. *83*, 7536–7546.

Sakuma, T., Noda, T., Urata, S., Kawaoka, Y., and Yasuda, J. (2009a). Inhibition of Lassa and Marburg virus production by tetherin. J. Virol. *83*, 2382–2385.

Sakuma, T., Sakurai, A., and Yasuda, J. (2009b). Dimerization of tetherin is not essential for its antiviral activity against Lassa and Marburg viruses. PLoS ONE *4*, e6934.

Sauter, D., Schindler, M., Specht, A., Landford, W.N., Münch, J., Kim, K.-A., Votteler, J., Schubert, U., Bibollet-Ruche, F., Keele, B.F., et al. (2009). Tetherin-driven adaptation of Vpu and Nef function and the evolution of pandemic and nonpandemic HIV-1 strains. Cell Host Microbe *6*, 409–421.

Schneider, T.R., and Sheldrick, G.M. (2002). Substructure solution with SHELXD. Acta Crystallogr. D Biol. Crystallogr. *58*, 1772–1779.

Sheldrick, G.M. (2002). Macromolecular phasing with SHELXE. Z. Kristallogr. *217*, 644–650.

Strebel, K., Klimkait, T., Maldarelli, F., and Martin, M.A. (1989). Molecular and biochemical analyses of human immunodeficiency virus type 1 vpu protein. J. Virol. *63*, 3784–3791.

Strebel, K., Luban, J., and Jeang, K.T. (2009). Human cellular restriction factors that target HIV-1 replication. BMC Med. *7*, 48.

Strelkov, S.V., and Burkhard, P. (2002). Analysis of alpha-helical coiled coils with the program TWISTER reveals a structural mechanism for stutter compensation. J. Struct. Biol. *137*, 54–64.

Svergun, D.I. (1992). Determination of the regularization parameter in indirect-transform methods using perceptual criteria. J. Appl. Cryst. *25*, 495–503.

Svergun, D.I. (1999). Restoring low resolution structure of biological macromolecules from solution scattering using simulated annealing. Biophys. J. *76*, 2879–2886.

Svergun, D.I., Petoukhov, M.V., and Koch, M.H. (2001). Determination of domain structure of proteins from X-ray solution scattering. Biophys. J. *80*, 2946–2953.

Terwilliger, T.C., and Berendzen, J. (1999). Automated MAD and MIR structure solution. Acta Crystallogr. D Biol. Crystallogr. *55*, 849–861.

Terwilliger, E.F., Cohen, E.A., Lu, Y.C., Sodroski, J.G., and Haseltine, W.A. (1989). Functional role of human immunodeficiency virus type 1 vpu. Proc. Natl. Acad. Sci. USA *86*, 5163–5167.

Van Damme, N., Goff, D., Katsura, C., Jorgenson, R.L., Mitchell, R., Johnson, M.C., Stephens, E.B., and Guatelli, J. (2008). The interferon-induced protein BST-2 restricts HIV-1 release and is downregulated from the cell surface by the viral Vpu protein. Cell Host Microbe *3*, 245–252.

Wriggers, W., Milligan, R.A., and McCammon, J.A. (1999). Situs: A package for docking crystal structures into low-resolution maps from electron microscopy. J. Struct. Biol. *125*, 185–195.

Zhang, F., Wilson, S.J., Landford, W.C., Virgen, B., Gregory, D., Johnson, M.C., Munch, J., Kirchhoff, F., Bieniasz, P.D., and Hatziioannou, T. (2009). Nef proteins from simian immunodeficiency viruses are tetherin antagonists. Cell Host Microbe *6*, 54–67.